Proceedings - 19th International Conference - IEEE/EMBS Oct. 30 - Nov. 2, 1997 Chicago, IL. USA

AN ALGORITHM THAT ESTIMATES BACKGROUND LUMIPHORE FOR LUMINESCENCE OPTICAL TOMOGRAPHY

J. Chang[1], H. L. Graber[2], R. L. Barbour[1,2]
Department of Pathology[1], and Program in Physiology and Biophysics[2]
SUNY Health Science Center at Brooklyn, Brooklyn NY 11203
Email: jchang@challenge.path.hscbklyn.edu

Abstract

We examine the impact of background lumiphore on image quality in luminescence optical tomography. A modification of a previously described algorithm [1,2] is developed that estimates the background luminescence directly from the detector readings. Numerical simulations were performed to calculate the diffusion–regime limiting form of forward–problem solutions for a specific test medium. Image reconstructions were performed with and without white noise added to the detector readings, using both the original and the improved versions of the algorithm. The results indicate that the original version produces unsatisfactory reconstructions when background lumiphore is present, while the improved algorithm yields qualitatively better images, especially for small target–to–background lumiphore ratios.

Key Words: luminescence, optical tomography, image reconstruction, range constraint.

1. Introduction

The use of lumiphore to enhance image quality in optical diffusion tomography has received considerable interest recently [1–5]. Luminescent compounds play a role in optical tomography analogous to that of radiopharmaceutical agents in nuclear medicine, in that both types of molecules actively emit photons from which projection or tomographic images are reconstructed. In an earlier paper [1] we described algorithms we have developed for reconstruction of two quantities of interest when the background scattering and absorption coefficients are known. These are the luminescence yield $\gamma\sigma_{a,l}N_0$ (*i.e.*, the product of the lumiphore's quantum yield, microscopic absorption cross section, and concentration) and the mean lifetime τ. We showed that $\gamma\sigma_{a,l}N_0$ can be reconstructed from DC (*i.e.*, steady–state, $\omega = 0$) detector readings. If detector readings for at least one $\omega \neq 0$ also are available, then they can in principle be used to reconstruct τ directly, without knowledge of $\gamma\sigma_{a,l}N_0$. However, for a numerical reason we adopted a "concentration correction" that makes use of the $\gamma\sigma_{a,l}N_0$ information while reconstructing τ. To implement this correction, the maximum value of each $\gamma\sigma_{a,l}N_0$ map is first obtained, and any value smaller than a threshold fraction of the maximum is set to zero. This modified $\gamma\sigma_{a,l}N_0$ map is then used in the calculation of the weight matrix (imaging operator) for the corresponding mean lifetime reconstruction. The examples we presented [1] showed that this concentration correction procedure works well in the absence of background lumiphore. Subsequently, however, we have seen that when background lumiphore is present, the reconstruction results are not satisfactory (see below).

One idea we have pursued in our efforts to deal with the problem just described is to make better use of *a priori* information in our image–reconstruction algorithms. It is well known that the use of *a priori* information is a powerful tool for finding the solutions of ill–conditioned problems [6]. For example, previous studies [7] have demonstrated that positivity constraints and range constraints can effectively improve image quality. However, great care must be taken to use range constraints properly, or they may not provide satisfactory results when background lumiphore is present. Background lumiphore not only significantly increases the detected signal, but also makes it difficult to assign a lower limit to the range constraint. An arbitrary choice of a lower bound (typically zero) is not satisfactory, as shown below in the results section. Thus, a requirement for successful reconstruction by our algorithms is a reasonable estimate of the background lumiphore concentration.

2. Reconstruction

In this study, a new procedure was developed to improve the reconstruction of concentration and mean lifetime when background lumiphore is present by directly estimating the background lumiphore's contribution from the detector readings. Here we

assumed that the background lumiphore is uniformly distributed with a constant concentration and mean lifetime, and that the target is an isolated object. Under these assumptions, the new procedure is:

1. Estimate the background luminescence yield (BLY) via the *maximum possible yield principle* (MPYP). This is a technique to compute a reasonable estimate *bly* of the (true) BLY from the DC detector readings. Suppose that all of the detected signal comes from background lumiphore. Since the BLY is constant, it is equal to the ratio of a detector reading to the corresponding weight function integrated over the entire volume of the medium. An estimate of BLY is obtained for each detector reading, and the lowest of these estimates is used as *bly*. BLY must be $\leq$ *bly*, since BLY > *bly* would imply negative contributions to the detector readings from the target.

2. Reconstruct $\gamma\sigma_{a,l}N_0$ using an iterative algorithm (*e.g.*, CGD, POCS, SART) with a range constraint where the upper and lower bounds respectively are the maximum possible target luminescence yield and *bly*. The former is estimated by supposing that all of the lumiphore added to the medium is concentrated in the target volume.

3. Re-estimate the BLY. That is, after reconstructing the targets from the initial *bly*, a new *bly* can be computed for use in the next reconstruction by subtracting the contribution of the reconstructed target from the detector readings. Repeated 1 to 3 until satisfactory *bly* is obtained.

4. Restrict the target volume by setting $\gamma\sigma_{a,l}N_0$ to *bly* in all voxels where $\gamma\sigma_{a,l}N_0 - bly$ is less than a preset fraction of $\max(\gamma\sigma_{a,l}N_0) - bly$.

5. Reconstruct the mean lifetime of the target and background. Here, we sum the weight function over all the background voxels so that the unknowns in this reconstruction are the voxels in the target plus one "lump" background voxel, thereby greatly reducing the dimension of the vector of unknowns.

3. Method

Numerical simulations were performed to calculate solutions to the diffusion equations describing the excitation and emission fields. The phantom was an infinite medium with background lumiphore uniformly distributed in an 8.0×8.0 cm^2 square region of interest (ROI) (Figure 1A). This area is discretized into 0.25× 0.25 cm^2 square voxels. The target was a smaller square located at the center of the ROI (Figure 1B). In the four

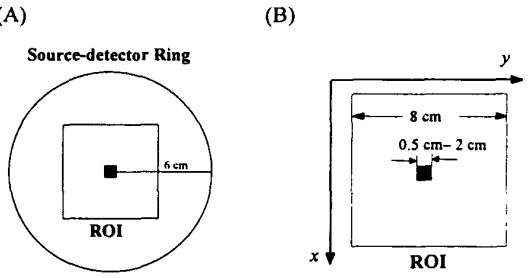

Figure 1. Sketches of phantom structure and source–detector ring used for diffusion computation.

test cases studied, the target size was: (A) 0.5 cm×0.5 cm, (B) 1.0 cm×1.0 cm, (C) 1.5 cm×1.5 cm, and (D) 2.0 cm×2.0 cm. The macroscopic cross sections for both excitation and emission light were $\mu_s = 1{,}000\ \mathrm{m}^{-1}$ and $\mu_a = 3\ \mathrm{m}^{-1}$. The absorption cross section introduced by the lumiphore was $\mu_{a,l} = 0.01\ \mathrm{m}^{-1}$. Two sets of mean lifetimes of the background and target lumiphore were tested. One is 5×10^{-9} s for the background and 10^{-9} s for the target. The other is 10^{-9} s for the background and 5×10^{-9} s for the target. Diffusion equation solutions were computed for DC illumination and for time–harmonic illumination at a modulation frequency of 100 MHz. These computations supplied the required information for reconstructions of luminescence yield and of mean lifetime. Different levels, defined as the ratio of the signal mean to the noise standard deviation, of Gaussian noise were also added to the detector readings. Images were obtained by using both the previously described [1] and improved versions of the reconstruction algorithm, both of which were terminated after 10,000 iterations.

4. Results

Figure 2 shows the reconstructed luminescence yield and mean lifetime when the background–to–target luminescence yield ratio was 0.01 and $\tau_{targ} < \tau_{back}$, for different target sizes, using the previously described algorithm with a positivity constraint on the luminescence yield and a 5×10^{-10} s to 5×10^{-9} s range constraint on the mean lifetime. (A) 0.5 cm×0.5 cm, (B) 1.0 cm×1.0 cm, (C) 1.5 cm×1.5 cm, and (D) 2.0 cm×2.0 cm. Figure 3 illustrates the reconstruction results when the background–to–target luminescence yield ratio was 0.2 and $\tau_{targ} < \tau_{back}$, for targets of different sizes, when the improved algorithm was used instead. The luminescence yield was constrained to lie between the maximum target value (0.05 m^{-1}) and the first *bly* selected by the algorithm. Figure 4 illustrates the reconstructed results for the same luminescence yield ratio as in Figure 3, but after the third estimate of BLY

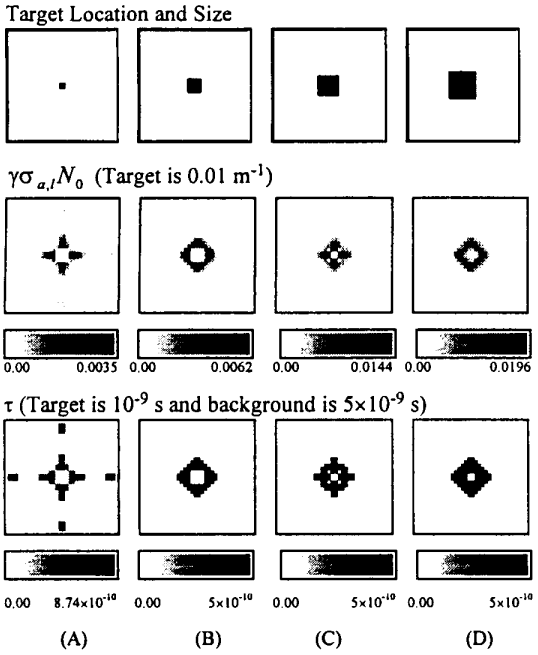

Figure 2. Reconstruction results with background–to–target luminescence yield ratio of 0.01 and different target sizes, using the previously described algorithm [1] with positivity constraints.

and with and $\tau_{targ} > \tau_{back}$. Figure 5 demonstrates the reconstruction results for a fixed background–to–target ratio of 0.01 and a fixed target size of 2.0 cm×2.0 cm, with different levels of added noise (1.0%, 3.0%, 5.0%, and 10.0%) and using the improved algorithm with constraints, after the first estimate of BLY.

5. Discussion and Conclusions

Our earlier report [1] described an algorithm that sequentially computes $\gamma\sigma_{a,l}N_0$ and τ using DC and AC data. (While neither sequential computation nor the use of different ωs is essential [3-5], we based our choice of these conditions on the different ω–dependence of detector sensitivity to changes in the quantities we reconstruct [2].) In the presence of background lumiphore, however, the original algorithm, which used a positivity constraint, failed to provide accurate quantitative results for either $\gamma\sigma_{a,l}N_0$ or τ (Figure 2). The algorithm set many voxels to zero while reconstructing $\gamma\sigma_{a,l}N_0$, instead of generating the uniform background we expected. It is likely that this is a consequence of the underdeterminedness of the weight matrix, which has infinitely many left–inverses, and that a uniform distribution does not lie on the fastest–converging path chosen by the algorithm. For a fixed target–to–background luminescence yield ratio, more accurate reconstructions were obtained for larger targets. This indicates that the background–to–target lumiphore ratio is not by itself a meaningful index of the difficulty of an image reconstruction problem, and the target size should be considered as well.

The reconstructions shown in Figures 3 and 4, produced by the revised algorithm, show significant improvement over those obtained from the original version, even though the background–to–target lumiphore ratio is twenty times larger in Figure 3 than in Figure 2. The qualitative and quantitative results are better after the third estimate of BLY (Figure 4) than after the first (Figure 3). The correlation of image quality with target size is not significant, or even becomes negative, because the BLY is accurately estimated using the MPYP. The size of the target, however, is underestimated for larger targets, while the quantitative values are overestimated. This is probably a consequence of the underdeterminedness of the weight matrix, and the error can be reduced by using regularization techniques [8–9]. In addition, the reconstructed mean lifetime is less accurate for larger objects because of the underestimated target size. The negative correlation between image quality and target size seems reasonable when we recall that the presence of a large target increases the detector readings appreciably above that due to the background. Thus, the BLY is overestimated by an amount depending on

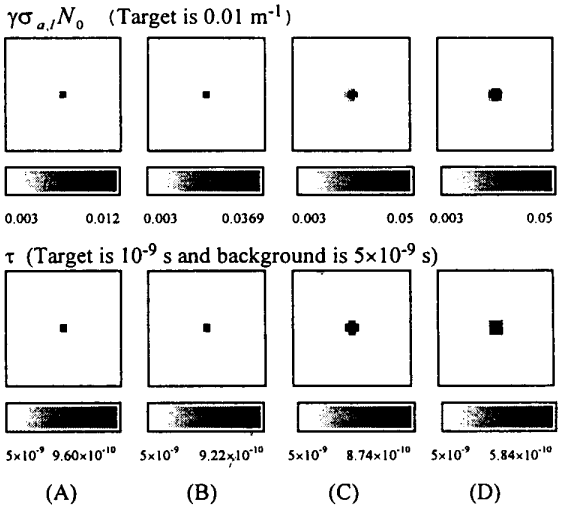

Figure 3. Reconstruction results with background–to–target lumiphore ratio of 0.2 and different target sizes, using the improved algorithm with range constraints, after the first estimate of BLY. Target locations and sizes are the same as for Figure 2, but background–to–target lumiphore ratio is 20 times larger.

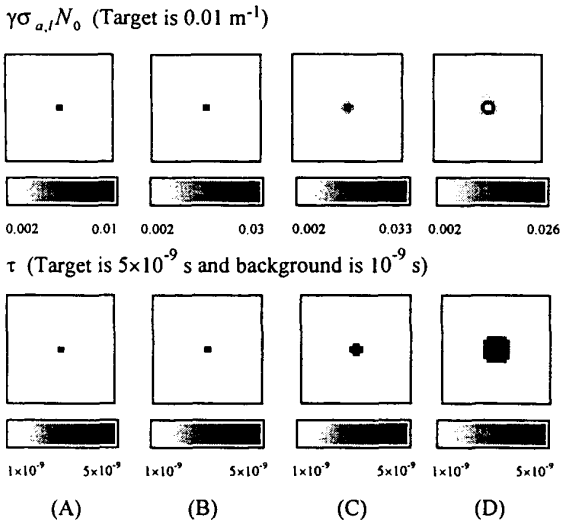

Figure 4. Reconstruction results with background–to–target lumiphore ratio of 0.2 and different target sizes, using the improved algorithm with range constraints and three-step estimate of BLY. Target locations and sizes are the same as for Figure 2.

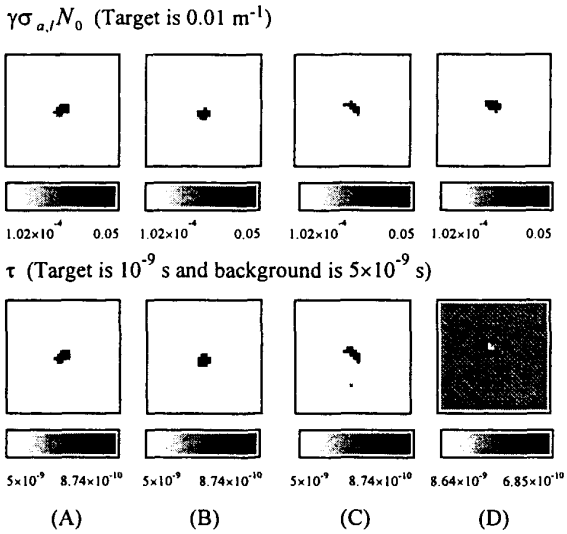

Figure 5. Reconstruction results with background–to–target ratio of 0.01 and different levels of added noise, with target size 2.0 cm×2.0 cm, and using the improved algorithm with range constraints, after the first estimate of BLY. (A) 1.0%, (B) 3.0%, (C) 5.0%, and (D) 10.0% noise.

the target's yield, size and location. High target yields, large targets, and targets located near sources or detectors result in significant overestimates of the BLY, thus distorting the reconstructed images.

The addition of noise distorted the reconstructed images in a noise–level–dependent manner. Results shown in Figure 5 demonstrate that reasonable qualitative accuracy was obtained from the improved algorithm even for 10% Gaussian noise added to the detector readings. The quantitative estimate of $\gamma\sigma_{a,l}N_0$ is inaccurate because of the noise. The mean lifetime values, however, are acceptable for up to 5% noise, even if the quantitative estimate of $\gamma\sigma_{a,l}N_0$ is incorrect. This is reasonable because $\gamma\sigma_{a,l}N_0$ is used only to delineate the target from the background. Its quantitative value is not important, because that is factored out in the mean lifetime reconstruction when computing the ratio of imaginary to real parts.

We acknowledge support from NIH grant RO1–CA59955 and RO1- CA66184-02.

6. References

1. J. Chang, H. L. Graber, and R. L. Barbour, "Luminescence optical tomography of dense scattering media," *J. Opt. Soc. Am. A*, vol. 14, pp. 288–299, 1997.
2. J. Chang, H. L. Graber, and R. L. Barbour, "Imaging of fluorescence in highly scattering media," *IEEE Trans. Biomed. Eng.* (in press)
3. Y. Paithankar, A. U. Chen, B. W. Pogue, M. S. Patterson, and E. M. Sevick–Muraca, "Imaging of fluorescent yield and lifetime from multiply scattered light reemitted from random media," *Applied Optics*, vol. 36, pp. 2260-2272, 1997.
4. J. Wu, Y. Wang, L. Perelman, I. Itzkan, R. R. Dasari, and M. S. Feld, "Three-dimensional imaging of objects embedded in turbid media with fluorescence and Raman spectroscopy," Applied Optics, vol. 34, pp. 3425-3430, 1995.
5. M. A. O'Leary, D. A. Boas, X. D. Li, B. Chance, and A. G. Yodh, "Fluorescence lifetime imaging in turbid media," *Optics Letters*, vol. 21, pp. 158–160, 1996.
6. D. C. Youla, "Mathematical theory of image reconstruction by the method of convex projections," *Image Recovery: Theory and Application*, Henry Stark, ed., Academic Press, New York, NY, 1987.
7. J. Chang, H. Graber, R. L. Barbour, and R. Aronson, "Recovery of optical cross section perturbations in dense scattering media using transport theory based imaging operators and steady–state simulated data and laser measurements," *Applied Optics* , vol. 35, pp. 3963–3978, 1996.
8. S. R. Arridge, "The forward and inverse problems in time resolved infra–red imaging," *Medical Optical Tomography: Functional Imaging and Monitoring*, SPIE Institutes, IS11, pp. 35–64, 1993.
9. J. Chang, W. Zhu, Y. Wang, H. L. Graber, and R. L. Barbour, "A regularized progressive expansion algorithm for recovery of scattering media from time–resolved data," *J. Opt. Soc. Am. A*, vol. 14, pp. 306–312, 1997.